3-2014

Revealing Interaction Of Organic Adsorbates With Semiconductor Surfaces Using Chemically Enhanced Raman

Andrew K. Kuhlman

Alexey T. Zayak
Bowling Green State University, azayak@bgsu.edu

THE JOURNAL OF PHYSICAL CHEMISTRY Letters

Letter

pubs.acs.org/JPCL

Revealing Interaction of Organic Adsorbates with Semiconductor Surfaces Using Chemically Enhanced Raman

Andrew K. Kuhlman and Alexey T. Zayak*

Department of Physics and Astronomy, Center for Photochemical Sciences, Bowling Green State University, Bowling Green, Ohio 43403, United States

Supporting Information

ABSTRACT: Surface enhanced Raman spectroscopy (SERS) is frequently associated with "chemical enhancement" (CE), which is an effect of the chemical coupling between reporting molecules and surfaces. While SERS technique is mainly attributed to the studies of metallic surfaces, chemical coupling must be present on semiconductor surfaces as well. Here, we examine binding of *trans*-1,2-two(4-pyridyl) ethylene (BPE) to various crystallographic facets of PbSe semiconductor. The calculated off-resonant Raman spectra vary significantly on different crystallographic facets of PbSe, correlating with the electronic structure of each type of semiconductor surface. We distinguish situations when the charge transfer is present and when it is not, which raises the question about what exactly should be called the "chemical enhancement". We attempt to clarify this situation by introducing the concept of the "charge-transfer" and "charge-transfer-less" chemical enhancement. We also demonstrate a transition between these two regimes, which exhibits a nonlinear behavior of the vibrational coupling and a significantly stronger contribution to the Raman intensity.

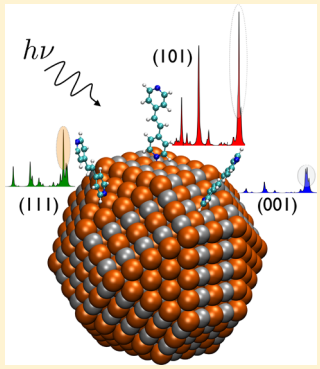

SECTION: Spectroscopy, Photochemistry, and Excited States

Since its discovery, SERS has shown significant promise for sensing individual molecules adsorbed near metal nanostructures or substrates with nanoscale roughness.[1−6] In SERS, the key aspect is that the incident light is collected by the nanoscale metallic structures and converted into plasmon excitations . This is a conversion from the far field regime to the near field, where optical density of states depends strongly on the distance from the metal nanoparticles. It is also typical that surface enhanced spectra look different from the corresponding solution Raman measurements,[7] which is due to the interfacial chemical interaction[8] and commonly referred to as the "Chemical Enhancement" (CE).[4,9]

A number of studies[10−17] have developed insightful and rather complex models that describe chemical interactions underlying CE. However, in a simplified view, CE can be rationalized in terms of the interfacial electronic structure energy level alignment between frontier molecular orbital energy and the metal Fermi energy, which sets the scale of the overall mode-independent multiplicative factor,[18] and quantifies the mode-specific degree to which a particular vibrational mode couples to the surface.[19] However, while on metals CE appears to be reasonably understood, modeling of CE on semiconductor surfaces is practically absent. Understanding of CE on semiconductors becomes even more important in the view of recent experimental studies.[20] In this paper, we explore the nature of CE on semiconductor surfaces.

Our computational model is the organic molecule trans-1,2-two(4-pyridyl) ethylene (BPE), that was previously used to investigate the nature of CE on silver and gold surfaces.[21−23] In this work, BPE is adsorbed to the surface of semiconductor PbSe. The rationale for choosing BPE is that the analogy with our previous work with gold will help us to understand the case of semiconductor surfaces. We focused on the three crystallographic facets, (001), (101), and (111), of the rock salt structure of PbSe.[24] The (001) facet of PbSe is convenient for computations, because it retains the well-defined semiconductor gap even without surface passivation. We want to avoid dealing with the surface passivation and reconstructions,[25,26] which would unnecesarily complicate our analysis.

DFT calculations were performed using the SIESTA code.[27] We used Perdew−Burke−Ernzerhof (PBE) parametrization for the XC-potential and double-ζ (DZP) basis set. Pseudopotentials for Pb, Se, N, C, and H were downloaded from the SIESTA web page. Crystallographic facets of the PbSe were represented by periodic slab geometries, with the corresponding crystallographic direction oriented along z-axis of the supercell. The in-plane lattice parameters of the PbSe slabs were kept according to the calculated bulk lattice constant, L = 6.29 Å, slightly larger than the experimental value of ≈6.124 Å,[28] which is expected when using the PBE XC-functional. The out-of-plane atomic coordinates of the slabs and the molecule were completely free to relax. Three different binding geometries for BPE on PbSe slabs are shown in Figure 1. A 2 × 2 × 1 Monkhorst-Pack k-points mesh was used for calculations involving PbSe slab; the Γ point was used for the isolated molecule calculations, and a 10 × 10 × 10 mesh was

Received: January 5, 2014
Accepted: February 27, 2014
Published: February 27, 2014

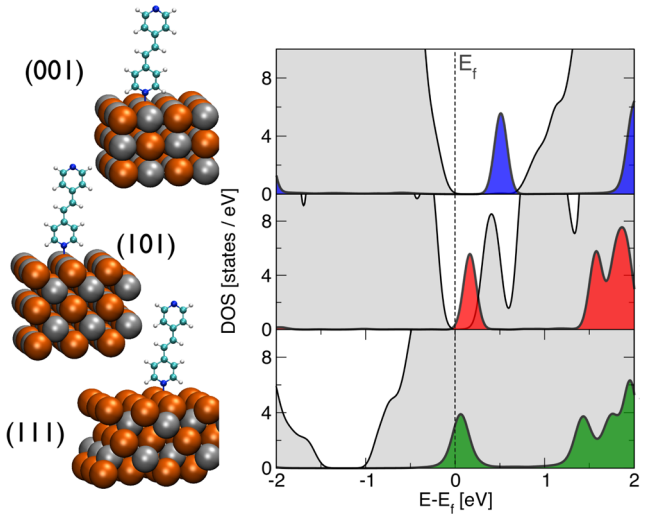

Figure 1. Left) Structural configurations of the three surfaces, (001), (101), and (111), with BPE molecule bound to Pb atom. (Right) Electronic density of states of the PbSe slabs and the molecular states, showing the position of the molecular LUMO relative to the Fermi level of the system.

used for the bulk PbSe calculations. The energy cutoff was set to 300 Ry in all calculations. Vibrations of the structures were computed by the method of Postnikov.[29] For the molecules adsorbed on the surfaces, Raman intensities are approximated by including only the R_{ZZ} component of the Raman tensor. The rationale for this approximation was discussed in our previous work.[19] We discussed that the chemical modification of the Raman signal should be the same for all Raman tensor components. By limiting our analysis to only R_{ZZ}, we obtain all information that is needed for our analysis. The DFT electronic level alignmnet in our work is only qualitatively meaningful. For a more quantitative picture, we would have to use a higher level theory,[30] which is left for future work.

In Figure 1, we summarize electronic structure information for three types of PbSe surfaces: (001), (101), and (111), with binding energies $E_{BPE(001)}$ = 0.06 eV, $E_{BPE(101)}$ = 0.12 eV and $E_{BPE(111)}$ = 0.22 eV, respectively. The density of states (DOS) plots show the distribution of PbSe states in the range of energies from −2 to 2 eV, centered at the Fermi level. The goal of this plot is to show the size of the energy gap in each case, as well as to locate the molecular electronic states relative to the semiconductor valence band maximum (VBM), or the Fermi level in a metallic system. In the case of the (001) surface, we see that the calculated semiconductor gap is about 0.5 eV. The lowest unoccupied molecular orbital (LUMO) of BPE landed in the semiconductor gap, slightly closer to the conduction band minimum (CBM). The combined (001) system has a gap of approximately 0.25 eV. The (101) surface, being less coordinated than (001) has a significantly smaller gap. The LUMO of BPE in this case is also in the gap, and leans toward the CBM. The last surface, (111), is metallic, which was made by design. The slab, which is used to represent this surface, is terminated by Pb atoms on both sides, which makes it strongly n-type. There is evidence that the (111) surface does not behave this way in reality. Instead, surface reconstructions are very likely to occur, allowing (111) to remain stoichiometric, and therefore less polar and nonmetallic.[24] In our case, we let the surface be metallic, because we want to have a metallic system for comparison.

Figure 2 addresses the issue of quantum confinement. We examine here the case of the (001) slab, while the (101) surface

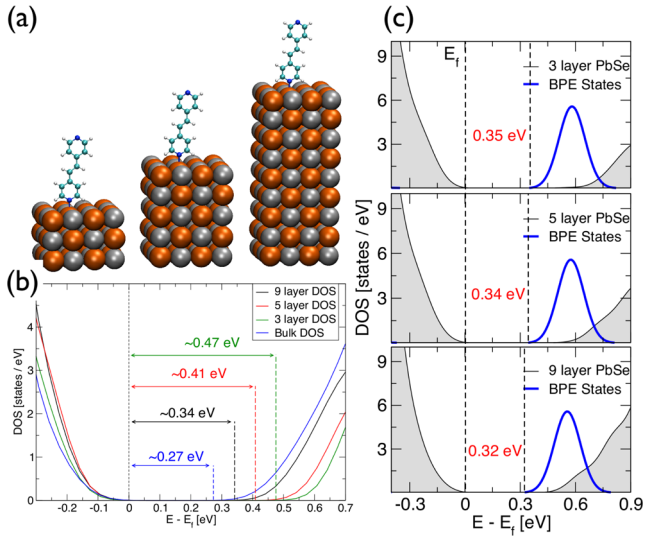

Figure 2. (a) Slab geometries in (001) orientation that are used to study the effect of quantum confinement in the Z-direction. (b) Density of states showing modification of the energy gap as a function of the slab thickness. (c) Density of states showing that the position of the LUMO relative to the Fermi level of the system is not affected by the quantum confinement.

has been checked too and showed similar behavior. The metallic (111) remains metallic at all thicknesses of the slab. While we see the quantum confinement effect on the energy gap between VBM and CBM, shown in Figure 2b, the distance between VBM and LUMO is practically unchanged. This indicates that the VBM-LUMO gap is mostly determined by the local chemistry at the binding site, with negligible effect from the confinement.

Our calculated Raman spectra are summarized in Figure 3. We show the same Raman data in two representations: the upper panel shows four Raman spectra plotted on the same vertical scale in order to emphasize the overall variations in the intensity on different surfaces; the lower panel shows the same Raman data, but the weaker signals have been multiplied, so that we could see differences in the shapes of the spectra. The Raman spectrum of the (101) surface shows the strongest overall signal, with 10 higher intensity than the (111) surface, and 20 times higher than the (001) surface. Clearly, the type of the surface significantly affects the interfacial Raman coupling.

With respect to the shape of the spectrum, we focus on the behavior of the two strongest peaks at 1595 cm^{-1} and 1631 cm^{-1}, highlighted in Figure 3c. According to Yang et al.,[21] the 1595 cm^{-1} mode has A_g symmetry and represents the pyridine ring C═C stretch, while the 1631 cm^{-1} mode also has A_g symmetry and represents the ethylenic C═C stretch (also shown graphically in SI). Previously, we discussed the behavior of these two peaks and their relation to CE.[22] It was shown that on a gold surface the relative intensities of these two peaks indicate the presence of chemical binding to the metal surface. If the 1595 cm^{-1} peak was slightly lower than the peak at 1631 cm^{-1}, then there was no direct chemical bonding between the molecule and the metal surface. On the other hand, if the 1595 cm^{-1} peak was much higher than 1631 cm^{-1}, then the Raman spectrum was said to be modified by CE.[22] The rationale for

dx.doi.org/10.1021/jz500024x | J. Phys. Chem. Lett. 2014, 5, 964−968

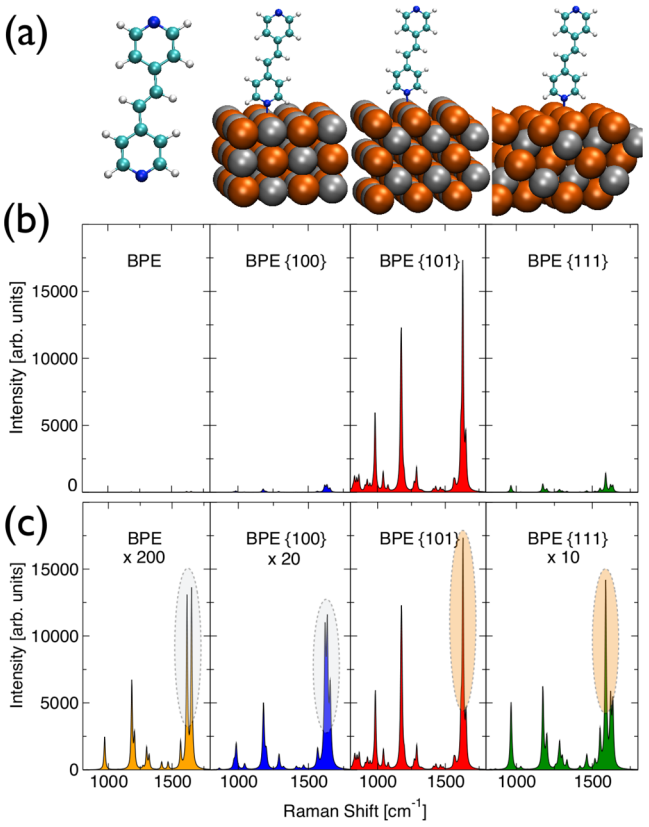

Figure 3. (a) Structural configurations for which Raman spectra are calculated. (b) Calculated Raman spectrum of BPE showing relative intensities on different surfaces. We note significantly stronger intensity on the (101) surface. (c) Raman spectra scaled up in order to show mode-specific features. The main feature is that only the (101) and (111) surfaces exhibit significant modification of the relative peaks intensities, strong enhancement of the 1595 cm^{-1} peak, reported previously on gold surfaces.[22]

this interpretation was that the 1595 cm^{-1} vibrational mode has larger deformation potential, yielding stronger charge transfer between gold surface and the bound molecule.[22]

Surprisingly, the spectrum of the (001) surface shows no significant change of the spectral shape, i.e., the spectrum looks very much like the one of the isolated BPE. While not changed in shape, this spectrum is still uniformly enhanced by about 10 times relative to the isolated BPE. Should we still call this "chemical enhancement"? Is CE only the change of the spectral shape or just the overall enhancement due to the chemical coupling, or both? Apparently, understanding of CE requires some additional terminology for clarification. We suggest referring to the (001) situation with the overall enhancement, but to no change of the spectral shape as "charge-transfer-less chemical enhancement" (CTL-CE), which will be discussed below.

On the other hand, the spectra of (101) and (111) surfaces clearly show changes of the shape (altered relative peaks intensities, as compared to the bulk spectrum), with much stronger peak at 1595 cm^{-1}.[22] We suggest to refer to the later situations as "charge-transfer chemical enhancement" (CT-CE), meaning that vibrational modes induce redistribution of charge across the molecule-surface interface.

The uniform enhancement of the signal on the (001) surface is due to the chemically modified lowest energy excitation that renormalizes the overall polarizability of the system. This mechanism had been investigated by Morton and Jensen, who indicated the absence of charge transfer.[18,31] If we express Raman signal by the two-state model,[31] then for a given vibrational mode Q_n we will have

$$R_{\alpha\beta}^{(n)} = \frac{\partial \chi_{\alpha\beta}}{\partial Q_n} \approx -\frac{M_\alpha^* M_\beta}{\omega_{\text{gap}}^2} \frac{\partial \omega_{\text{gap}}}{\partial Q_n} \quad (1)$$

where $R_{\alpha\beta}^{(n)}$ is the Raman tensor component, $\chi_{\alpha\beta}$ is the electronic polarizability, M_α and M_β are the transition dipole moments, which are assumed to be independent from Q_n.[18,31] The overall Raman enhancement on the (001) surface has to be attributed only to the renormalization of ω_{gap}^2 in the denominator of eq 1. While, the derivative, $\partial\omega_{\text{gap}}/\partial Q_n$, which we call "deformation potential" (see Supporting Information (SI) for more information), has to be the same as for the isolated molecule, otherwise the relative peaks intensities would change. Indeed, this is exactly what we see in our direct analysis of the deformation potential presented in the SI. In the case of BPE, the deformation potential is the shift of the LUMO relative to the VBM of PbSe.

Our (111) surface is metallic, and the spectrum is not only enhanced, but also exhibits a significantly modified profile, very similar to the case of the Au(111) surface.[22] The displacements of the LUMO in this case cause crossing of E_{Fermi}, which drives the interfacial charge redistribution.[19] The mechanism of the electron-vibration coupling is "anharmonic" in this case, meaning that the charge transfer is effectively damping the amplitude of the LUMO shift, which is reflected by the deformation potential (see detailed analysis in the SI).

Thus, the (001) and (111) surfaces allow us to demonstrate two types of the chemical enhancement: CTL-CE and CT-CE. In the first case, the coupling of the vibrations with the interfacial electronic structure is "harmonic", because it does not involve the charge transfer. On the other hand, the CT-CE mechanism exhibits renormalized amplitude of the LUMO shift (deformation potential), which is due to the "anharmonic" character of the process. It is the anharmonic case that leads to the modification of the relative peak intensities in chemically enhanced Raman spectra, as compared to bulk intensities (i.e isolated molecule). Distinguishing these two regimes of CE might be very handy in the future studies of surface Raman spectroscopy.

Finally, we focus on the anomalously strong Raman signal on the (101) surface.We expected the strongest signal from the metallic surface (111), because the (111) surface has the largest polarizability (see Figure 4a). However, instead, the (101) surface shows Raman intensity 10 times higher than (111). The 1595 cm^{-1} peak on (101) has also been enhanced, which means that we have the CT-CE regime with charge transfer. In Figure 4a, we examine how the electronic polarizability, χ, changes as a function of the vibrational amplitude, Q_n, associated with the 1595 cm^{-1} mode for all surfaces and for the isolated BPE. The overall scale of the polarizability of each structure correlates very nicely with the binding energy of BPE to the surface (see Figure 6 in the SI). However, more importantly, the (101) case shows a uniquely nonlinear behavior of the polarizability. The almost linear trends in other cases mean that if there is charge transfer, it happens at approximately constant rate when the LUMO moves up or down, $\partial\rho/\partial Q_n \approx$ const, where ρ is the occupation of the LUMO. In the case of the (101) surface, the charge transfer changes nonlinearly, as shown in Figure 4. We see that when

dx.doi.org/10.1021/jz500024x | J. Phys. Chem. Lett. 2014, 5, 964−968

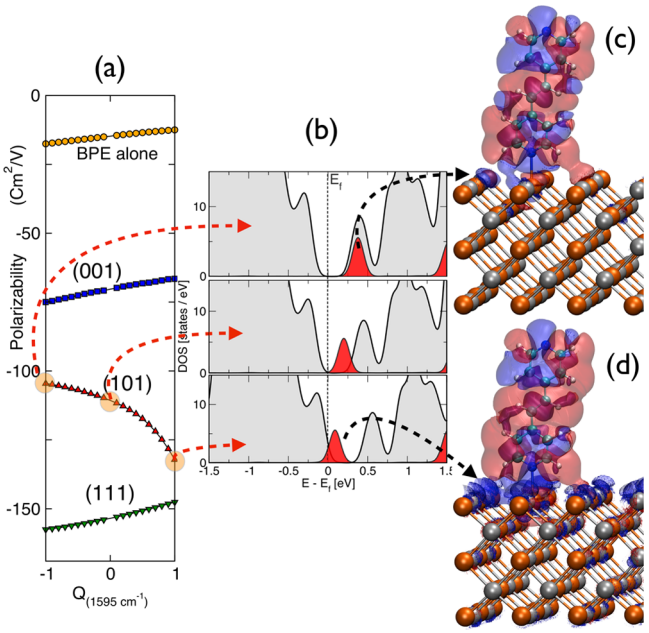

Figure 4. (a) Electronic polarizability calculated for the isolated BPE and three PbSe surfaces with BPE, plotted against the scaled amplitude, $Q_{1595cm^{-1}}$, of the 1595 cm^{-1} mode. Polarizability of the (101) shows clearly nonlinear behavior when LUMO starts crossing the Fermi level. (b) Density of electronic states of the (101) surface, showing the change of the LUMO position as a function of the vibrational displacement in mode at 1595 cm^{-1}. The shift of LUMO is not symmetric. (c,d) Differences in the charge density induced by the displacement of LUMO shown in panel b. In the case of panel d, we see that lowering of the LUMO below E_{Fermi} causes charge depletion on the surface of PbSe (the cloud on the surface means missing charge, relative to the equilibrium geometry).

the LUMO goes down, it crosses the Fermi level, becoming more occupied. When the LUMO goes up, the semiconductor gap only increases, without causing any charge redistribution. Thus, the vibrational coupling to the electronic structure of the (101) surface is rectified. This anomaly is related to the fact that the system is right at the border between the metallic and semiconducting state. The vibrational dictortion is able to drive the transition between the two regimes, indicated by the change in the slope of the polarizability curve in Figure 4, which is the crossover between the CT-CE and CTL-CE deformation potential. In Figure 4c,d, two isosurfaces in different colors show charge depletion and charge accumulation caused by the vibration at 1595 cm^{-1}. No cloud means nothing changes relative to the equilibrium geometry. When the LUMO goes down in energy, we see a significant amount of charge density disappearing from the surface of the semiconductor (the cloud on the surface in Figure 4d shows the missing charge). At the same time, the absence of such cloud in Figure 4c means that nothing changes on the surface when the LUMO goes up.

In summary, we observed that binding to the semiconductor surfaces significantly affects Raman spectra of organic adsorbates, but on each surface in a different way. Overall, the two-state model provides adequate basis for an intuitive understanding of the interfacial contribution to Raman. However, the behavior of the electron-vibration coupling at the interface needs to be clarified in each case. We suggest that by introducing the terms of "charge-transfer-chemical-enhancement" (CT-CE) and "charge-transfer-less-chemical-enhancement" (CTL-CE), we can differentiate between the situations when vibrations induce interfacial charge transfer and when they do not, respectively. Although our calculations are done in the approximation of the infinite wavelength, they should provide useful basis for the future TD-DFT calculations, which will reveal the wavelength dependent nature of the CT-CE and CTL-CE regimes. The transition between these two regimes implies the possibility of turning "on" and "off" the vibration-induced charge transfer by changing the excitation wavelength, which can lead to novel types of Raman measurements, directly probing electronic structure of the crystal-molecule interfaces.

■ ASSOCIATED CONTENT

Supporting Information

The Supporting Information contains additional data that is used to support the analysis of this work. This material is available free of charge via the Internet at http://pubs.acs.org/.

■ AUTHOR INFORMATION

Corresponding Author

*E-mail: azayak@bgsu.edu.

Notes

The authors declare no competing financial interest.

■ ACKNOWLEDGMENTS

We thank BGSU for startup funds and IT support, and the Texas Advanced Computer Center (TACC) and XSEDE (project TG-DMR130080) and the Ohio Supercomputer Center (startup project PCS0220) for computational resources. A.T.Z. thanks Pierre Darancet and Elena I. Liskova for helpful discussions. We thank our reviewer for suggesting the CT-CE and CTL-CE nomenclature.

■ REFERENCES

(1) Fleischman, M.; Hendra, P. J.; McQuillan, A. Raman Spectra of Pyridine at a Silver Electrode. *Chem. Phys. Lett.* **1974**, *26*, 163.
(2) Jeanmaire, D. L.; Duyne, R. P. V. Surface Raman Spectroelectrochemistry: Part 1: Heterocyclic, Aromatic, and Aliphatic Amines Adsorbed on the Anodized Silver Electrode. *J. Electroanal. Chem.* **1977**, *84*, 1−20.
(3) Albrecht, M. G.; Creighton, J. A. Anomalously Intense Raman Spectra of Pyridine at a Silver Electrode. *J. Am. Chem. Soc.* **1977**, *99*, 5215.
(4) Moskovits, M. Surface-Enhanced Spectroscopy. *Rev. Mod. Phys.* **1985**, *57*, 783.
(5) Willets, K. A.; Duyne, R. P. V. Localized Surface Plasmon Resonance Spectroscopy and Sensing. *Annu. Rev. Phys. Chem.* **2007**, *58*, 267−297.
(6) Stiles, P. L.; Dieringer, J. A.; Shah, N. C.; Van Duyne, R. P. Surface-Enhanced Raman Spectroscopy. *Annu. Rev. Anal. Chem.* **2008**, *1*, 601−626.
(7) Otto, A.; Billmann, J.; Eickmans, J.; Ertürk, U.; Pettenkofer, C. The "Adatom Model" of SERS (Surface Enhanced Raman Scattering): The Present Status. *Surf. Sci.* **1984**, *138*, 319−338.
(8) Moskovits, M. Persistent Misconceptions Regarding SERS. *Phys. Chem. Chem. Phys.* **2013**, *15*, 5301.
(9) Campion, A.; Kambhampati, P. Surface-Enhanced Raman Scattering. *Chem. Soc. Rev.* **1998**, *27*, 241.
(10) Jensen, L.; Aikens, C. M.; Schatz, G. C. Electronic Structure Methods for Studying Surface-Enhanced Raman Scattering. *Chem. Soc. Rev.* **2008**, *37*, 1061−1073.
(11) Lombardi, J. R.; Birke, R. L.; Lu, T.; Xu, J. Charge-Transfer Theory of Surface-Enhanced Raman Spectroscopy. *J. Chem. Phys.* **1986**, *84*, 4174−4180.
(12) Heller, E. J.; Sundberg, R. L.; Tannor, D. Simple Aspects of Raman Scattering. *J. Phys. Chem.* **1982**, *86*, 1822−1833.

(13) Arenas, J. F.; Tocón, I. L.; Otero, J. C.; Marcos, J. I. Charge Transfer Processes in Surface-Enhanced Raman Scattering: Franck–Condon Active Vibrations of Pyridine. *J. Phys. Chem.* **1996**, *100*, 9254–9261.
(14) Adrian, F. J. Charge Transfer Effect in Surface-Enhanced Raman Scattering. *J. Chem. Phys.* **1982**, *77*, 5302.
(15) Persson, B. N. J.; Zhao, K.; Zhang, Z. Chemical Contribution to Surface-Enhanced Raman Scattering. *Phys. Rev. Lett.* **2006**, *96*, 207401.
(16) Lombardi, J. R.; Birke, R. L. A Unified Approach to Surface-Enhanced Raman Spectroscopy. *J. Phys. Chem. C* **2008**, *112*, 5605–5617.
(17) Lombardi, J. R.; Birke, R. L. The Theory of Surface-Enhanced Raman Scattering. *J. Chem. Phys.* **2012**, *136*, 144704.
(18) Morton, S. M.; Jensen, L. Understanding the Molecule-Surface Chemical Coupling in SERS. *J. Am. Chem. Soc.* **2009**, *131*, 4090.
(19) Zayak, A. T.; Hu, Y. S.; Choo, H.; Bokor, J.; Cabrini, S.; Schuck, P. J.; Neaton, J. B. Chemical Raman Enhancement of Organic Adsorbates on Metal Surfaces. *Phys. Rev. Lett.* **2011**, *106*, 083003.
(20) Islam, S. K.; Tamargo, M.; Moug, R.; Lombardi, J. R. Surface-Enhanced Raman Scattering on a Chemically Etched ZnSe Surface. *J. Phys. Chem. C* **2013**, *117*, 23372–23377.
(21) Yang, W.-h.; Hulteen, J.; Schatz, G. C.; Van Duyne, R. P. A Surface-Enhanced Hyper-Raman and Surface-Enhanced Raman Scattering Study of trans-1,2-bis(4-pyridyl)ethylene Adsorbed onto Silver Film over Nanosphere Electrodes. Vibrational Assignments: Experiment and Theory. *J. Chem. Phys.* **1996**, *104*, 4313.
(22) Zayak, A. T.; Choo, H.; Hu, Y. S.; Gargas, D. J.; Cabrini, S.; Bokor, J.; Schuck, P. J.; Neaton, J. B. Harnessing Chemical Raman Enhancement for Understanding Organic Adsorbate Binding on Metal Surfaces. *J. Phys. Chem. Lett.* **2012**, *3*, 1357–1362.
(23) Mohammed, A.; Hu, W.; Andersson, P. O.; Lundquist, M.; Landström, L.; Luo, Y.; Ågren, H. Cluster Approximations of Chemically Enhanced Molecule-Surface Raman Spectra: The Case of trans-1,2-bis (4-pyridyl)ethylene (BPE) on Gold. *Chem. Phys. Lett.* **2013**, *581*, 70–73.
(24) Fang, C.; van Huis, M. A.; Vanmaekelbergh, D.; Zandbergen, H. W. Energetics of Polar and Nonpolar Facets of PbSe Nanocrystals from Theory and Experiment. *ACS Nano* **2010**, *4*, 211–218.
(25) Huang, X.; Lindgren, E.; Chelikowsky, J. Surface Passivation Method for Semiconductor Nanostructures. *Phys. Rev. B* **2005**, *71*, 165328-1.
(26) Leitsmann, R.; Bechstedt, F. Characteristic Energies and Shifts in Optical Spectra of Colloidal IV–VI Semiconductor Nanocrystals. *ACS Nano* **2009**, *3*, 3505–3512.
(27) Soler, J. M.; Artacho, E.; Gale, J. D.; Garcia, A.; Junquera, J.; Ordejon, P.; Sanchez-Portal, D. The SIESTA Method for Ab-Initio Order-N Materials Simulation. *J. Phys.: Condens. Matter* **2002**, *14*, 2745.
(28) Ramasamy, K.; Nejo, A. O.; Ziqubu, N.; Rajasekhar, P. V. S. R.; Nejo, A. A.; Revaprasadu, N.; O'Brien, P. A New Route to Lead Chalcogenide Nanocrystals. *Eur. J. Inorg. Chem.* **2011**, *2011*, 5196–5201.
(29) Postnikov, A. V.; Pages, O.; Hugel, J. Lattice Dynamics of the Mixed Semiconductors (Be,Zn)Se from First-Principles Calculations. *Phys. Rev. B* **2005**, *71*, 115206.
(30) Yu, M.; Doak, P.; Tamblyn, I.; Neaton, J. B. Theory of Covalent Adsorbate Frontier Orbital Energies on Functionalized Light-Absorbing Semiconductor Surfaces. *J. Phys. Chem. Lett.* **2013**, *4*, 1701–1706.
(31) Jensen, L.; Zhao, L. L.; Autschbach, J.; Schatz, G. C. Theory and Method for Calculating Resonance Raman Scattering from Resonance Polarizability Derivatives. *J. Chem. Phys.* **2005**, *123*, 174110.